Applied Surface Science 605 (2022) 154696

Contents lists available at ScienceDirect

Applied Surface Science

journal homepage: www.elsevier.com/locate/apsusc

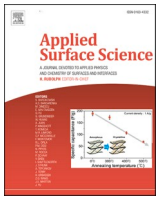

Full Length Article

Heteropolyacids supported on zirconia-doped γ, θ and α alumina: A physicochemical assessment and characterisation of supported solid acids

Luke Forster [a,*], Zhipeng Qie [a,b], Min Hu [a], Aristarchos Mavridis [a], Cameron Price [a,c], Christopher M.A. Parlett [a,c,d,e], Xiaolei Fan [a,f], Carmine D'Agostino [a,g,*]

[a] Department of Chemical Engineering, School of Engineering, The University of Manchester, Oxford Road, Manchester M13 9PL, United Kingdom
[b] Faculty of Environment and Life, Beijing University of Technology, Beijing 100124, China
[c] Catalysis Hub, Research Complex at Harwell, Rutherford Appleton Laboratory, Oxfordshire OX11 0FA, United Kingdom
[d] Diamond Light Source Ltd, Harwell Science and Innovation Campus, Didcot, Oxfordshire OX11 0DE, United Kingdom
[e] University of Manchester at Harwell, Diamond Light Source, Didcot, Oxfordshire OX11 0DE, United Kingdom
[f] Nottingham Ningbo China Beacons of Excellence Research and Innovation Institute, 211 Xingguang Road, 315191, Ningbo, China
[g] Dipartimento di Ingegneria Civile, Chimica, Ambientale e dei Materiali (DICAM), Alma Mater Studiorum – Università di Bologna, Via Terracini, 28, 40131 Bologna, Italy

ARTICLE INFO

Keywords:
Heterogeneous Catalysis
Heteropolyacids
Alumina
Surface Chemistry
Low-Field NMR
NMR Relaxation

ABSTRACT

In this paper we carry out a surface study of promising supported solid acid catalysts commonly used for the production of high value chemicals derived from glycerol. In particular, γ, θ and α alumina (Al_2O_3) were modified by (i) grafting with 5 wt% zirconia, (ii) doping with 30 wt% silicotungstic acid (STA), and (iii) using both zirconia and STA. The aim is to rationalise the effect of these different parameters on structural properties and surface adsorption through a comprehensive multi-technique approach, including recently developed NMR relaxation techniques. XRD and laser Raman spectroscopy confirmed a strong interaction between STA and the γ-/θ-Al_2O_3 resulting in a distortion of the supported STA Keggin structure relative to that of bulk STA. Conversely, a much weaker interaction between the supported STA and α-Al_2O_3 was measured. NMR relaxation demonstrated that the STA doping increases the adsorption properties of the catalyst, particularly for γ-/θ-Al_2O_3. For catalysts based on α-Al_2O_3, such effect was negligible. Thermogravimetric/differential thermogravimetry (TGA/DTG) analysis suggested that zirconia-grafted and non-grafted θ-Al_2O_3 and γ-Al_2O_3 are suitable materials for increasing the thermal stability of STA whereas α-Al_2O_3 (both grafted and non-grafted) does not improve the thermal stability of STA.

1. Introduction

As crude oil prices continue to increase and supplies become scarcer, it is increasingly apparent that new processes based on renewable feedstocks must be developed for more sustainable production of chemicals and materials. Biofuels (e.g., bio-diesel) are widely regarded as one of the most promising renewable feedstock and as such their production has increased dramatically in recent years. In fact, biofuels and advanced biofuels are projected to account for >17% of total demand for transport fuels by 2050 [1]. Production of 1st and 2nd generation fatty acid methyl esters (the most common biodiesels) results in the generation of large amounts of raw glycerol (50–70% purity, 10 kg per 100 kg of biodiesel) as the main by-product. In the UK and Ireland alone, 58 ktons of waste glycerol is produced annually, which is either incinerated on-site or sent to make fertilizers and biogas [2]. Due to the massive abundance of glycerol produced and the relatively high amount of glycerol that is wasted, many efforts have been made to find ways of upgrading glycerol to value-added platform chemicals such as acrolein [3].

Acrolein is a key intermediate produced from glycerol dehydration and is commonly used at very low concentrations as a biocide for water treatment to limit the growth of aquatic weeds in irrigation waterways [4] or in the oil and gas industries as a biocide in oil-field brines [5]. Arguably the most important application of acrolein, however, is as an intermediate to the production of acrylic acid *via* catalytic oxidation [6]. Acrylic acid is a key bulk chemical used as an intermediate for the

* Corresponding authors at: Department of Chemical Engineering, School of Engineering, The University of Manchester, Oxford Road, Manchester M13 9PL, United Kingdom (C. D'Agostino).
E-mail addresses: luke.forster@manchester.ac.uk (L. Forster), carmine.dagostino@manchester.ac.uk, carmine.dagostino@unibo.it (C. D'Agostino).

https://doi.org/10.1016/j.apsusc.2022.154696
Received 24 June 2022; Received in revised form 3 August 2022; Accepted 26 August 2022
Available online 1 September 2022

production of many valuable chemicals and materials, such as in various polymers and coatings [7]. Global production of acrylic acid from crude oil is currently in excess of several million metric tons annually [8,9] and this is increasing by 3 – 5% every year [10]. As such, it should be clear that the production of acrylic acid by sustainable processes, such as the catalysed oxidation of acrolein produced by waste glycerol dehydration, is highly desirable in terms of creating a circular economy using sustainable processes.

For the dehydration of glycerol to take place effectively, acidic species are required [11–13]. Due to their relative ease of separation, solid, heterogeneous acid catalysts are generally desirable from an industrial perspective. As such, the development of such catalysts is an important area of research. One such class of materials attracting much research interest are heteropolyacids (HPAs), such as silicotungstic acid (STA) [12,14,15]. HPAs are highly acidic and generally considered as green catalysts [16] but possess a relatively low surface area and porosity [17,18]. In order to circumvent these issues, HPAs are generally dispersed on supports with relatively high surface areas, thermal stability and porosities [18]. Porous silica [19], zirconia [20,21], and alumina [22,23] have been used for this purpose amongst others [24–26]. The nature of the support will significantly change the nature of the resultant catalyst, through both chemical and physical means. Therefore, elucidation of support effects is of vital importance for an effective catalyst design and few studies have so far been reported in this area.

Recent studies have demonstrated both the effectiveness of HPAs supported on aluminas doped with different metals (particularly zirconia) [27] and the significant impact that the alumina phase has on the overall catalysts effectiveness by changing various catalyst properties [28]. This study aims to gain in-depth knowledge of these materials using a variety of characterisation techniques to determine the effect of alumina phase on the textural, structural and chemical properties of zirconia doped-alumina supported STA catalysts.

2. Experimental

2.1. Materials

Materials were used as delivered, without any additional purification, unless otherwise specified: γ, θ, and α-Al_2O_3 (Johnson Matthey), *n*-octane (Merck), pyridine (Sigma-Aldrich), silicotungstic acid hydrate (STA, $H_4SiW_{12}O_{40}{\cdot}18H_2O$, Sigma-Aldrich), zirconyl (IV) nitrate hydrate ($ZrO(NO_3)_2{\cdot}6.8H_2O$, Sigma-Aldrich). Deionised water was obtained from a laboratory water purification system.

2.2. Synthesis of solid catalysts

A typical preparation was carried out to prepare 5 g of catalyst. The catalyst preparation method is based on that of a previously reported study [28]. Silicotungstic acid (STA, 30 wt%, 1.500 g, 4.675×10^{-4} mol) was dissolved in an appropriate volume of water and supported on to each different alumina phase using an incipient wetness impregnation method. The appropriate volume of aqueous STA solution to completely fill the pores of γ, θ, and α-Al_2O_3, respectively, was added to the appropriate support and the resultant slurry was stirred for 20 h. The slurry was then dried at 110 °C for 16 h in static air.

Zirconia (5 wt%) was grafted to each alumina support by dissolving the appropriate mass of zirconyl (IV) nitrate hydrate (0.933 g, 7.350×10^{-4} mol) in deionised water (~10 mL). The desired alumina support was mixed with deionised water (10 mL) and the aqueous metal salt solution was added dropwise to the alumina slurry with stirring at 60 °C until a semi-solid paste was formed. The resultant paste was dried at 110 °C for 3 h before calcination at 500 °C for 3 h using a ramp rate of 6 °C min^{-1} from room temperature.

STA (30 wt%) was supported on the zirconia grafted alumina supports using an incipient wetness impregnation method. STA (1.500 g, 4.675×10^{-4} mol) was dissolved in deionised water to prepare an appropriate volume of aqueous STA solution to completely fill the pores of the desired support. The resultant slurry was stirred for 20 h before drying at 110 °C for 16 h in static air.

2.3. N_2 adsorption-desorption analysis

N_2 physisorption analysis was performed at −196 °C by using either an automatic 3H-2000 PM2 analyzer (Beishide Co. Ltd) or Quantachrome Quadrasorb Evo. Before N_2 adsorption measurements, ~250 mg of samples were degassed at 300 °C for 6 h. Isotherms and total pore volume (V_p) were directly measured from the instrument. Total specific surface areas (S_a) were calculated from isotherms based on the Brunauer-Emmett-Teller (BET) theory. Pore size analysis was obtained from the desorption branch of the obtained isotherms using the BJH method.

2.4. XRD

X-ray diffraction patterns were obtained using a Bruker D8 Discover diffractometer equipped with a Cu K-alpha1 source and Lynxeye XE-T detector. The samples were scanned from 5-80° 2θ in 0.02 ° steps, with a count time of 1 s per step.

2.5. Laser Raman spectroscopy measurements

Raman spectra were obtained using a Horiba LabRAM spectrometer equipped with a 488 nm excitation laser. Spectra were obtained between the wavenumbers of 200 cm^{-1} and 1800 cm^{-1}.

2.6. NMR relaxation 2D T_1-T_2 correlation analysis

Catalyst particles (~100 mg) were soaked in *n*-octane or pyridine for 2 days prior to analysis. The particles were removed from the respective liquids and gently dried on a pre-soaked filter paper to remove excess liquid from the outer surface whilst avoiding removal of liquid from the internal pore structure.

Following drying, the catalyst samples were transferred to 5 mm NMR tubes and tested using a T_1-T_2 NMR pulse sequence (Figure 1) to determine spin-lattice and spin-spin relaxation times. The typical error for all T_1-T_2 measurements was approximately 3 %.

Sixteen recovery delays were used, from 500 ms to 5000 ms. The echo train of the CPMG sequence was composed between 64 and 1200 echoes dependent upon the sample acquired, in a single shot with an echo spacing of $2\tau = 1$ ms. Each data set was acquired with 4 scans in approximately 2 min. The 2D data was processed using a Laplace inversion algorithm previously developed [29].

2.7. TGA/DTG analysis

TGA/DTG analyses were performed using a thermograviemtric analyser (TGA 550) in the temperature range 30 – 800 °C with a heating rate of 10 °C/min^{-1} in a flow of N_2 (60 mL min^{-1}).

3. Results and discussion

3.1. N_2 adsorption-desorption analysis

The different phases of Al_2O_3 are known to have numerous differences both in terms of textural and chemical properties. Both textural and chemical differences, and indeed a combination of both, can have a significant impact upon the catalytic activity and selectivity when multiple different catalytic materials are considered for the same process. Textural differences will generally impact mass transport processes whereas chemical differences will usually influence the different adsorption and desorption processes and chemical transformations

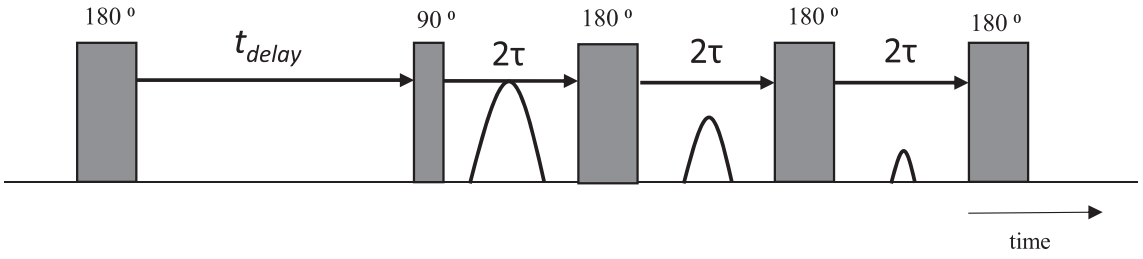

Fig. 1. T_1-T_2 NMR pulse sequence. The thin and thick vertical bars represent 90° and 180° radiofrequency (RF) pulses, respectively. T_1 relaxation is encoded in the variable time t_{delay}. T_2 relaxation is encoded in the train of n 180° pulses. A single data point is acquired at the centre of each echo time, τ.

taking place on the surface of the catalytic materials.

To assess the impact of the Zr and STA doping upon the textural properties of the alumina materials studied, N_2 adsorption-desorption analysis was performed on all of the materials studied, the results of which can be seen in Table S1.

The first point to note is that the average pore size, d_{pore}, increases in the order γ-Al_2O_3 > θ-Al_2O_3 > α-Al_2O_3 whereas the surface area, S_a, decreases in the same order. This is typical of these alumina phases and is commonly reported for such materials [30,31].

Generally, d_{pore} and S_a decrease slightly with each doping treatment, which can be attributed to deposition of dopants within the pores of the support, thereby reducing the average pore diameter and overall surface area.

3.2. X-ray diffraction measurements

Whilst it is indeed important to assess the changes in physical and textural parameters of these materials, it is also important to determine the nature of the interaction between the dopants (Zr and STA) and the alumina surface. As such, the catalysts were characterised using X-ray diffraction (Figure 2).

The XRD patterns for 30STA-α and 30STA-5Zr-α (Figure 2c and 2d for α-Al_2O_3) showed distinct reflections typical of bulk STA (Figure S1a, *ca.* 10°-20° and *ca.* 25°-35°). The presence of bulk STA peaks (Figure S1a) in the 30STA-α and 30STA-5Zr-α diffraction patterns suggests a poor distribution of STA on the α-Al_2O_3 surface which, in turn, suggests a weak interaction between STA and α-Al_2O_3. However, it is important to note that this could also be due to the build-up of large STA clusters on the α-Al_2O_3 surface as 30 wt% STA is spread over a relatively small surface area. When the diffraction patterns of the γ-Al_2O_3 and θ-Al_2O_3 catalysts are considered, only the broad diffraction peaks characteristic of γ-Al_2O_3 and θ-Al_2O_3 are present, respectively. Therefore, XRD measurements can be seen as a clear indication that STA has a greater degree of dispersion over γ-Al_2O_3 and θ-Al_2O_3 than when compared to α-Al_2O_3.

Similarly, when the diffraction patterns of 5Zr-γ, 5Zr-θ and 5Zr-α are considered (Figure 2b), there is little to no change in the diffraction pattern when compared to that of the pure aluminas. Again this would suggest a high degree of dispersion of zirconia on the alumina surface as peaks indicative of bulk zirconia (Figure S1b) are not seen in the diffraction pattern. The same is true of the diffraction patterns of 30STA-5Zr-γ, 30STA-5Zr-θ and 30STA-5Zr-α which would seem to further support the presence of dispersed Zr on the catalyst surfaces. It is possible that mixed oxide phases may be present, however, these are not detected by XRD and further work would be required to determine their presence.

3.3. Laser Raman spectroscopy measurements

To investigate the nature of the interaction between STA and the different alumina phases Raman spectroscopy was performed. Laser Raman spectroscopy has been shown to be capable of both confirming the presence of the catalytically active Keggin structure of STA and the strength of the interaction between the Keggin species and the support surface [14]. The presence of the Keggin species can be confirmed by the presence of the characteristic peak in the Raman spectra at *ca.* 1000 cm^{-1} [32]. Such a peak is present in the Raman spectra of all STA doped catalysts (Figure 3) indicating that the Keggin species of STA is present on all catalyst surfaces. Bands characteristic of Keggin structure STA are; ~1000 cm^{-1} attributed to the W=O stretch and ~974 cm^{-1} to W-O-W bending [14,32,33].

It is interesting to note the difference in the Keggin signature bands between the catalysts made using different alumina phases. In the catalysts with greater STA dispersion (γ-Al_2O_3 and θ-Al_2O_3 as evidenced by

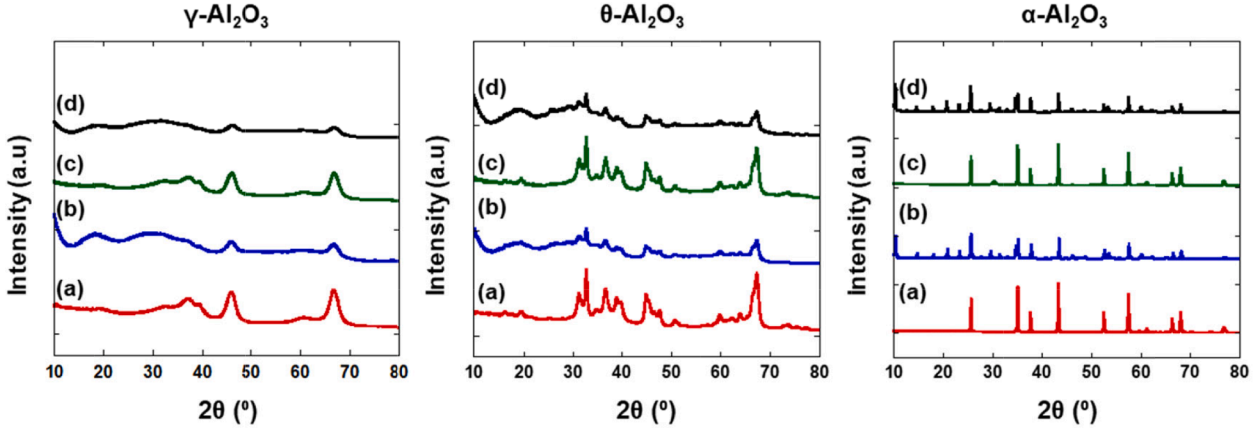

Fig. 2. X-ray diffraction patterns of (a) pure phase alumina, (b) alumina doped with 30 wt% STA, (c) alumina doped with 5 wt% Zr and (d) alumina doped with both 5 wt% Zr and 30 wt% STA. Alumina phases are shown above their respective diffraction patterns.

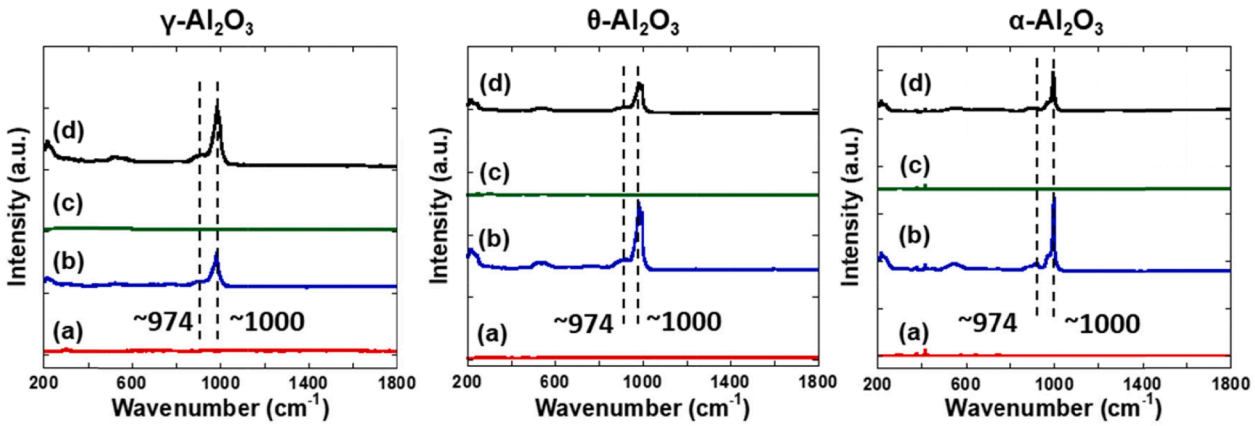

Fig. 3. Laser Raman spectra of (a) pure phase alumina, (b) alumina doped with 5 wt% Zr, (c) alumina doped with 30 wt% STA and (d) alumina doped with both 5 wt % Zr and 30 wt% STA. Alumina phases are shown above their respective Raman spectra. An excitation laser with a wavelength of 488 nm was used.

XRD) it can be seen that the W-O-W bending shoulder peak at 974 cm^{-1} is merged with the W=O stretch peak at 998 cm^{-1}. This has previously been attributed to a slight distortion and bond weakening of the Keggin species resulting from a strong binding between the Keggin structure and the support [28]. This peak merging is more prevalent in the γ-Al_2O_3 catalyst Raman spectra indicating that the strongest STA-surface interactions are achieved when γ-Al_2O_3 is used as support. The opposite is true of α-Al_2O_3 and θ-Al_2O_3 is intermediate between the two.

3.4. NMR relaxation 2D T_1-T_2 correlation measurements

Whilst the textural and structural properties of a supported solid acid catalyst for alcohol dehydration is essential to their performance, it is of course vital to also consider the chemical properties of such materials. Arguably the most important chemical factor to consider is the interaction with the acid sites of the catalysts, as the alcohol group must be protonated to be removed from the reactant for dehydration.

NMR relaxation measurements have been shown to be a fast, easy and non-destructive method of determining relative liquid molecule-solid surface interaction strengths of guest molecules imbibed within porous media (i.e. catalytic materials) [34–38] to unravel and explain various relevant phenomena occurring during catalytic processes. Recently such measurements have been used to determine the acidity of solid catalysts [39,40]. As such, NMR relaxation measurements using pyridine, which is commonly used as a probe molecule to measure the acidity of a solid catalyst [41–43], were performed on the catalysts studied. The plots obtained can be seen below in Figure 4 and results obtained seen in Table S2.

Whilst the individual relaxation times can be determined from the peaks in Figure 4, it is T_1/T_2 that has been shown to be an effective measurement of the strength of interaction between a guest molecule (in this case pyridine) and a solid surface [44]. In brief, the greater the value of T_1/T_2, the stronger the interaction between the guest molecule and the surface. Pyridine is basic in nature so will interact strongly with strong acidic sites on the catalyst surface. Therefore, it follows that a relatively high T_1/T_2 of pyridine confined within the pores of the catalysts studied will indicate a surface with relatively strong acidity. It is important to note that T_1/T_2 of pyridine confined within the pores of the catalysts is generally indicative of the strength of interaction with the catalyst surface [45]. However, T_1/T_2 is effectively a measure of the surface interaction which will be weighted towards the strongest sites of pyridine adsorption. Therefore, an increase in acid site density can also indirectly be reflected in T_1/T_2 [39].

The results of these measurements can be visualised graphically below in Figure 5.

In the pure/non-doped aluminas, the relative acid site strength of both γ-Al_2O_3 and θ-Al_2O_3 is approximately the same. In the case of non-doped α-Al_2O_3, the acidity is much higher than the other phases. This is consistent with previous measurements on the acidity of single alumina phases and further confirms the utility of this technique [46].

Upon doping with 30 wt% STA, the relative strength of acidity of γ and θ phase alumina is increased considerably whereas there is little to no increase in the acidity of the α phase. In combination with the findings of XRD and Raman, this suggests that a strong interaction between the alumina surface and STA, as well as presence of the Keggin structure on the alumina surface, leads to catalytic materials with a higher acidity. Therefore, a key conclusion is that it is important to maximise the interaction between STA and the support surface to produce catalysts with a high acidity to facilitate effective dehydration performance. In the α-Al_2O_3 doped with 30 wt% STA, bulk STA is present on the Al_2O_3 surface (shown by XRD, Figure 2) and it is clear that the lack of interaction between the two makes little difference to the strength of acidity of the resultant material.

Upon doping with 5 wt% Zr, there is very little change in the strength of acidity relative to the non-doped aluminas. However, when the Zr-doped aluminas are subsequently doped with 30 wt% STA, there is a substantial increase in acid strength relative to both the non-doped aluminas and those doped with STA only. This would suggest that the presence of the Zr monolayer on the alumina surfaces acts to enhance the interaction between the support and STA thereby increasing the acidity of the resultant catalyst. Similarly to the alumina doped with 30 wt% STA only, the γ and θ phase materials are approximately the same in terms of acid site strength whereas α is weaker. Again, this can be attributed to the strength of interaction between the STA and alumina support as discussed previously.

The addition of Zr and STA to alumina in this way has previously been theorised to modify catalyst acidity by weakening the acidity of STA [14,28,47]. It has been suggested that during catalyst preparation, hydroxyl groups on the surface of metal oxide supports (i.e. Al_2O_3, ZrO_2, SiO_2) are protonated forming M-OH_2^+ groups. These groups interact with the heteropolyanion [48] and the strength of this interaction is thought to influence the Brønsted acidity of the supported HPA, where a stronger interaction will distort the Keggin structure, thereby decreasing the HPA acid strength [14,28,47].

The grafting of zirconia has previously been shown to tune the catalyst acidity to between −2 and −8 on the Hammett acidity (HA) scale, which is favourable for the formation of acrolein from glycerol [49,50]. Again, this is due to an increased interaction strength between the hetreopolyanion and the support resulting in a Keggin structure distortion and a decreased overall acidity. This has been proven for mixed phase δ, θ-Al_2O_3 and for α-Al_2O_3 supported HPA catalysts [28]. Therefore, the results reported herein appear to suggest that the interaction between STA and non-grafted γ-Al_2O_3 and θ-Al_2O_3 is weaker than the interaction between STA and zirconia-grafted γ-Al_2O_3 and θ-Al_2O_3

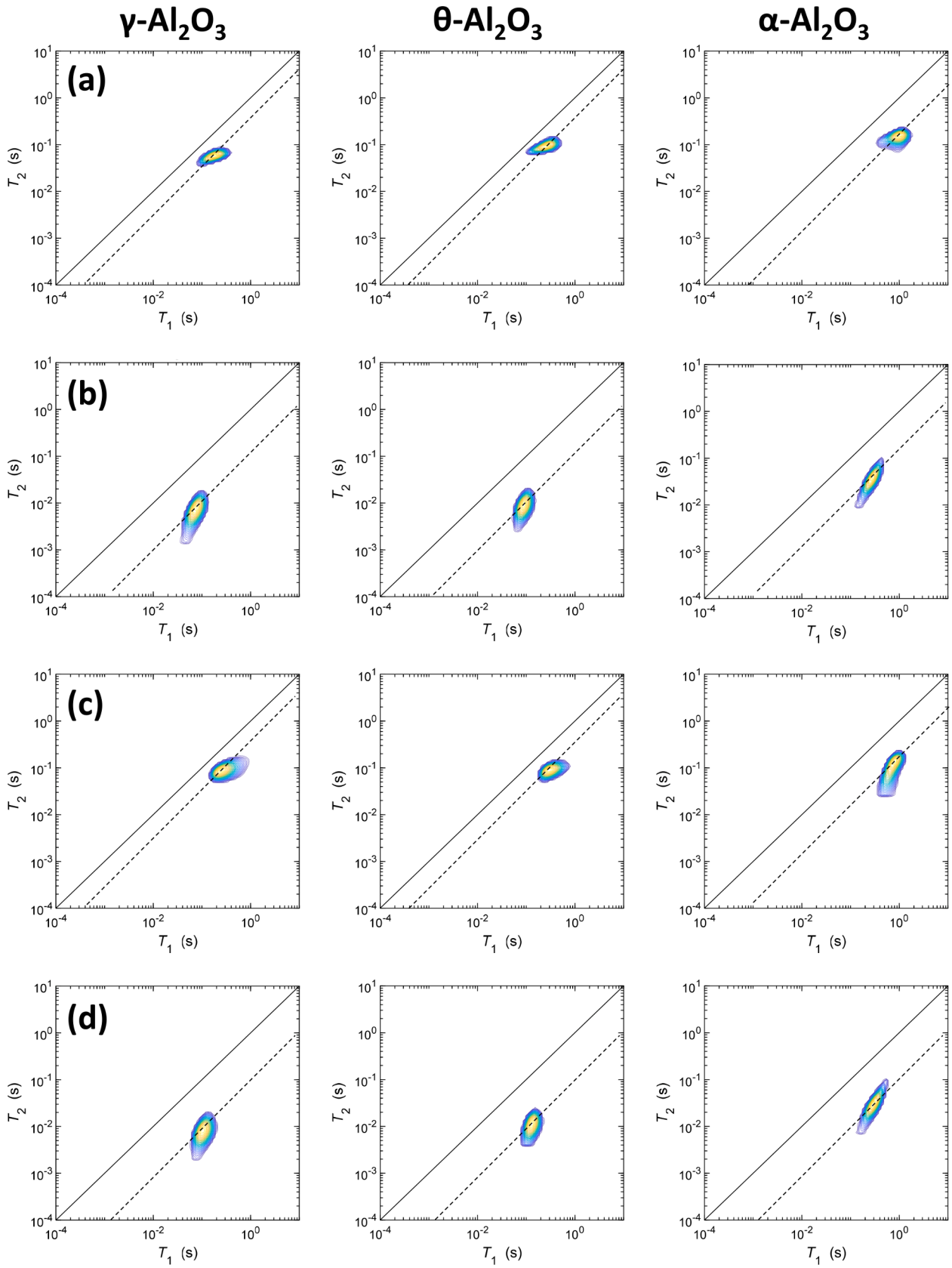

Fig. 4. 2D T_1-T_2 correlation plots obtained using pyridine imbibed within the pores of (a) pure phase alumina, (b) alumina doped with 5 wt% Zr, (c) alumina doped with 30 wt% STA and (d) alumina doped with both 5 wt% Zr and 30 wt% STA. Alumina phases are shown above their respective plots. The black line represents $T_1 = T_2$. Dashed black lines indicate the peak maxima where T_1/T_2 is calculated from.

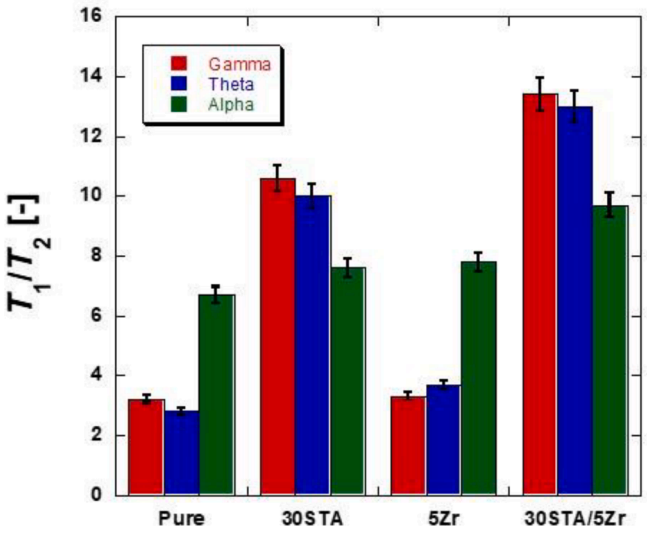

Fig. 5. T_1/T_2 measured using pyridine imbibed within the pores of the catalysts studied. A high T_1/T_2 indicates a relatively strong acid site is present on the catalyst surface.

thereby the overall acidity is increased upon doping the support with STA. The interaction of STA with α-Al_2O_3 is minimal (as shown by XRD, Fig. 2) therefore this effect is less pronounced and no significant changes in acidity are detected.

It is important to note the differences in acidity determination between the acidity determination techniques and previous similar work. NH_3-TPD is commonly used to measure the acidity of such materials and when compared to pyridine NMR relaxation measurements there are significant differences between these two methods, although there is a proven correlation between the two [39,44]. The use of a liquid probe molecule (pyridine) as opposed to a gaseous probe molecule (ammonia), their relative differences in basicity, confinement effects (relevant in NMR relaxation measurements) and the use of elevated temperatures (room temperature for NMR relaxation whereas higher temperatures are used for NH_3-TPD) can possibly contribute to differences in results between the two techniques.

3.5. Thermogravimetric analysis

One limitation to the use of heteropolyacids, such as STA, as effective catalysts for the dehydration of glycerol to acrolein, is their relatively poor thermal stability. Analysis of the TGA-DTG data for bulk STA (Figure S2) shows three clear regions of weight loss. The weight loss at 77 °C occurs due to the desorption of physisorbed water whilst the weight loss at 203 °C occurs due to the loss of crystalline water from the STA structure. The third region of weight loss at 469 °C is related to the decomposition of the STA Keggin structure. The different steps of STA thermal decomposition can be seen in Scheme 1.

Deposition of heteropolyacids upon the surface of support materials has previously been shown to improve the thermal stability of heteropolyacids, particularly, the thermal stability of the Keggin structure [21,51,52]. To investigate the impact of the alumina phase upon this increased STA thermal stability, TGA-DTG data were collected, the results of which can be seen in Fig. 6.

Firstly, it should be noted that, in terms of overall weight loss, the materials studied generally had thermal stabilities in the order; α-Al_2O_3 > θ-Al_2O_3 > γ-Al_2O_3. This is typical of differing aluminas phases with α-Al_2O_3 being the most thermally stable of the phases and γ-Al_2O_3 the least.

Secondly, DTG thermograms for the θ-Al_2O_3 and γ-Al_2O_3 samples show two broad peaks at *ca.* 70 °C and 355 °C, which are attributed to the loss of physisorbed water and structural water, respectively [21,51,52]. Most importantly, the DTG thermograms show no significant change in the rate of weight loss at temperatures above 400 °C. As the Keggin structure decomposes at temperatures above 500 °C (Figure S2), this indicates that the STA Keggin structure is retained at high temperatures when supported on θ and γ-Al_2O_3 and therefore the overall thermal stability of STA is increased. When the α-Al_2O_3 catalysts are considered, the DTG profile is similar to that of the bulk STA (Figure S2) with 3 peaks seen at *ca.* 54 °C, 163 °C and 445 °C, respectively, attributed to the loss of physisorbed water, structural crystalline water and the decomposition of the Keggin structure respectively. This would suggest that the thermal stability of STA is not improved when supported on α-Al_2O_3 (both zirconia-grafted and non-grafted), most likely due to the poor dispersion of STA on the α-Al_2O_3 (as shown by XRD, Figure 2) and weak interaction between the heteropolyanion and α-Al_2O_3 surface (as shown by Raman, Figure 3).

4. Conclusions

Several phases of alumina, γ, θ and α, were grafted with 5 wt% zirconia and then doped with 30 wt% silicotungstic acid (STA). The different phase aluminas were also doped with 30 wt% STA without zirconia grafting. Several characterisation techniques were performed on the listed catalytic materials to fully assess the textural and chemical properties of the alumina catalytic materials.

Textural and structural properties of the catalytic materials were determined using N_2 adsorption-desorption analysis. This suggested the presence of a zirconia monolayer on the support surface, which enhances the thermal stability of the catalytic materials by suppressing high temperature phase transformations thereby maintaining a high catalytic surface area, which can be beneficial for catalysis. N_2 adsorption-desorption analysis confirmed blockage of the support pores upon doping with STA, resulting in an overall loss of surface area, pore volume and average pore diameter.

X-ray diffraction measurements confirmed a strong interaction between STA and γ and θ-Al_2O_3 (both zirconia grafted and non-grafted) whilst the presence of bulk STA on the surface of α-Al_2O_3 suggested little to no interaction between STA and this alumina support. The lack of diffraction peaks indicative of bulk zirconia across all diffraction patterns confirmed a good dispersion of zirconia across the alumina surfaces.

Laser Raman spectroscopy provided further confirmation of the strong interaction between both γ and θ-Al_2O_3 (grafted and non-grafted) and STA, which results in a distortion of the STA Keggin structure. The strength of this interaction was shown to be of the order $\alpha < \theta \leq \gamma$ regardless of zirconia grafting.

NMR relaxation measurements using pyridine imbibed within the catalyst pores demonstrated that doping the alumina supports with STA significantly increased catalyst acidity whereas grafting with zirconia had no significant impact on the overall acidity of the resultant catalytic material. Subsequent doping of the zirconia-grafted aluminas with STA resulted in catalysts with an increased acidity relative to those prepared using the non-grafted aluminas for the γ and θ phase alumina supported catalysts whereas the effect on α phase alumina materials was negligible. The increase in acidity seen is due to a greater interaction between non-

$$H_4[SiW_{12}O_{40}]\bullet nH_2O \xrightarrow[>200\ °C]{-nH_2O} H_4SiW_{12}O_{40} \xrightarrow[>500\ °C]{-2H_2O} SiW_{12}O_{38} \longrightarrow 12WO_3 + SiO_2$$

Scheme 1. The thermal decomposition of STA with increasing temperature.

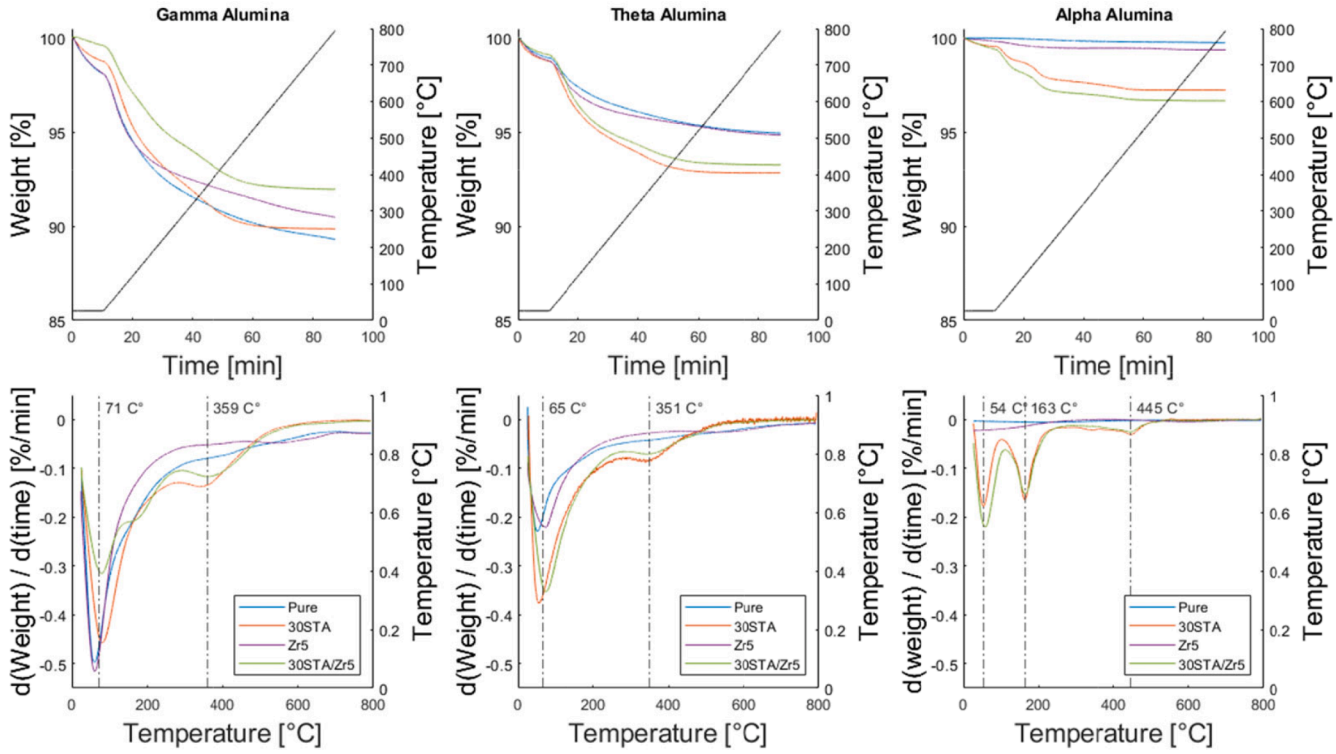

Fig. 6. TGA-DTG thermograms of the prepared catalytic materials.

grafted γ and θ phase alumina and the STA heteropolyanion when compared to the equivalent zirconia-grafted materials. This increased interaction strength distorts the STA Keggin structure thereby reducing the relative overall catalyst acidity.

TGA-DTG analysis suggested that zirconia-grafted and non-grafted θ-Al_2O_3 and γ-Al_2O_3 are suitable materials for increasing the thermal stability of STA. The catalytically active Keggin heteropolyanion structure was preserved at temperatures greater than 400 °C, where it would otherwise be expected to decompose when unsupported. α-Al_2O_3 showed significant decomposition of the STA Keggin structure at *ca.* 445 °C indicating that it is not a suitable support for increasing the thermal stability of STA. This was thought to occur due to the presence of bulk STA on the α-Al_2O_3 surface owing to the relatively weak interaction between the heteropolyanion and the α-Al_2O_3 surface as well as the relatively poor dispersion of STA on this support material.

Data availability

The data that supports the findings of this study is available within the article and the supporting information.

CRediT authorship contribution statement

Luke Forster: Data curation, Formal analysis, Visualization, Methodology, Investigation, Writing – original draft, Writing – review & editing. **Zhipeng Qie:** Data curation, Formal analysis, Visualization, Writing – review & editing. **Min Hu:** Data curation, Formal analysis. **Aristarchos Mavridis:** Data curation, Formal analysis. **Cameron Price:** Data curation, Formal analysis, Writing – review & editing. **Christopher M.A. Parlett:** Writing – review & editing, Supervision, Resources. **Xiaolei Fan:** Writing – review & editing, Supervision, Resources. **Carmine D'Agostino:** Conceptualization, Methodology, Visualization, Supervision, Funding acquisition, Writing – review & editing.

Declaration of Competing Interest

The authors declare that they have no known competing financial interests or personal relationships that could have appeared to influence the work reported in this paper.

Acknowledgements

L.F. and C.D. would like to acknowledge the EPSRC (EP/V026089/1) for supporting their research activities.

The author(s) acknowledges the use of the Department of Materials X-ray Diffraction Suite at the University of Manchester and is grateful for the technical support and data collected by Gary Harrison.

C.A.M.P and C.A.H.P would like to thank the Research Complex for access and support to these facilities and equipment. In addition the UK Catalysis Hub is kindly thanked for resources and support provided via our membership of the UK Catalysis Hub Consortium and funded by EPSRC grant EP/R027129/1.

Appendix A. Supplementary data

Supplementary data to this article can be found online at https://doi.org/10.1016/j.apsusc.2022.154696.

References

[1] D. Chiaramonti, G. Talluri, N. Scarlat, M. Prussi, The Challenge of Forecasting the Role of Biofuel in EU Transport Decarbonisation at 2050: A Meta-Analysis Review of Published Scenarios, Renew. Sust. Energ. Rev. 139 (2021), 110715, https://doi.org/10.1016/j.rser.2021.110715.

[2] M. Pagliaro, Glycerol the Renewable Platform Chemical, first ed., Elsevier, Amsterdam, 2017.

[3] R. Beerthuis, G. Rothenberg, N.r. Shiju, Catalytic Routes Towards Acrylic Acid, Adipic Acid and ε-caprolactam Starting From Biorenewables, Green Chem. 17 (2015) 1341–1361, https://doi.org/10.1039/C4GC02076F.

[4] J. van Overbeek, W.J. Hughes, R. Blondeau, Acrolein for the Control of Water Weeds and Disease-Carrying Water Snails Science, 129 (1959), pp. 335–336, 10.1126/science.129.3345.33.

[5] D. Arntz, A. Fischer, M. Höpp, S. Jacobi, J. Sauer, T. Ohara, T. Sato, N. Shimizu. H. Schwind, Acrolein and Methacrolein in; Ullmann's Encyclopaedia of Industrial Chemistry Wiley-VCH, Weinheim, 2007, 10.1002/14356007.a01_149.pub2.

[6] T.v. Andrushkevich, Heterogeneous Catalytic Oxidation of Acrolein to Acrylic Acid: Mechanism and Catalysts, Catal. Rev. Sci. Eng. 35 (1993) 213–259, https://doi.org/10.1080/01614949308014606.

[7] T. Oharo, T. Sato, N. Shimizu, G. Prescher, H. Schwind, O. Weiberg, K. Marten, H. Greim, T.D. Shaffer, P. Nandi, Acrylic Acid and Derivatives in; Ullmann's Encyclopaedia of Industrial Chemistry Wiley-VCH, Weinheim, 2020, 10.1002/14356007.a01_161.pub4.

[8] J.G.H. Hermens, A. Jensma, B.L. Feringa, Highly Efficient Biobased Synthesis of Acrylic Acid, Angew. Chem. Int. Ed. 61 (2022) e202112618, 10.1002/anie.202112618.

[9] A. Niesbach, R. Fuhrmiester, T. Keller, P. Lutze, A. Górak, Esterification of Acrylic Acid and *n*-Butanol in a Pilot-Scale Reactive Distillation Column—Experimental Investigation, Model Validation, and Process Analysis, Ind. Eng. Chem. Res. 51 (2012) 16444–16456, https://doi.org/10.1021/ie301934w.

[10] A. Godefroy, G.S. Patience, T. Tzakova, D. Garrait, J.-l. Dubois, Reactor Technologies for Propane Partial Oxidation to Acrylic Acid, Chem. Eng. Technol. 32 (2009) 373–1370, https://doi.org/10.1002/ceat.200800309.

[11] W. Suprun, M. Lutecki, T. Haber, H. Papp, Acidic Catalysts for the Dehydration of Glycerol: Activity and Deactivation, J. Mol. Catal. A Chem. 309 (2009) 71–78, https://doi.org/10.1016/j.molcata.2009.04.017.

[12] L. Liu, B. Wang, Y. Du, A. Borgna, Supported $H_4SiW_{12}O_{40}/Al_2O_3$ Solid Acid Catalysts for Dehydration of Glycerol to Acrolein: Evolution of Catalyst Structure and Performance with Calcination Temperature, Appl. Catal. A-Gen. 489 (2015) 32–41, https://doi.org/10.1016/j.apcata.2014.10.017.

[13] G.S. Foo, D. Wei, D.S. Sholl, C. Sievers, Role of Lewis and Brønsted Acid Sites in Dehydration of Glycerol over Niobia, ACS Catal. 4 (2014) 3180–3192, https://doi.org/10.1021/cs5006376.

[14] H. Atia, U. Armbruster, A. Martin, Dehydration of Glycerol in Gas Phase Using Heteropolyacid Catalysts as Active Compounds, J. Catal. 258 (2008) 71–82, https://doi.org/10.1016/j.jcat.2008.05.027.

[15] Z. Wang, L. Liu, Mesoporous Silica Supported Phosphotungstic Acid Catalyst for Glycerol Dehydration to Acrolein, Catal. Today 376 (2021) 55–64, https://doi.org/10.1016/j.cattod.2020.08.007.

[16] M. Misono, Acid Catalysts for Clean Production: Green Aspects of Heteropolyacid Catalysts, C. R. Acad. Sci. Paris, Series IIc: Chem. 3 (2000) 471–475, https://doi.org/10.1016/S1387-1609(00)01165-8.

[17] M.G. Kulkarni, R. Gopinath, L.C. Meher, A.k. Dalai, Solid acid catalyzed biodiesel production by simultaneous esterification and transesterification, Green Chem. 8 (2006) 1056–1062, https://doi.org/10.1039/B605713F.

[18] M.A. Hanif, S. Nisar, U. Rashid, Supported Solid and Heteropolyacid Catalysts for Production of Biodiesel, Catal. Rev. 59 (2017) 165–188, https://doi.org/10.1080/01614940.2017.1321452.

[19] E. Tsukuda, S. Sato, R. Takahashi, T. Sodesawa, Production of Acrolein from Glycerol over Silica-Supported Heteropolyacids, Catal. Comm. 8 (2007) 1349–1353, https://doi.org/10.1016/j.catcom.2006.12.006.

[20] B. Viswanadham, A. Srikanth, K.v.r. Chary, Characterization and Reactivity of 11-Molybdo-1-Vanadophosphoric Acid Catalyst Supported on Zirconia for Dehydration of Glycerol to Acrolein, J. Chem. Sci. 126 (2014) 445–454, https://doi.org/10.1007/s12039-014-0586-z.

[21] A. Talebian-Kiakalaieh, N.a.s. Amin, Supported Silicotungstic Acid on Zirconia Catalyst for Gas Phase Dehydration of Glycerol to Acrolein, Catal. Today 256 (2015) 315–324, https://doi.org/10.1016/j.cattod.2015.01.045.

[22] L. Cheng, X.p. Ye, A DRIFTS Study of Catalyzed Dehydration of Alcohols by Alumina-Supported Heteropolyacid, Catal. Lett. 130 (2009) 100–107, https://doi.org/10.1007/s10562-009-9887-0.

[23] E. Kraleva, R. Palcheva, L. Dimitrov, U. Armbruster, A. Brückner, A. Spojakina, Solid Acid Catalys for Dehydration of Glycerol to Acrolein in Gas Phase, J. Mater. Sci. 46 (2011) 7160–7168, https://doi.org/10.1007/s10853-011-5379-x.

[24] B. Visawanadham, N. Nagaraju, C.N. Rohitha, V. Vishwanathan, K.v.r. Chary, Synthesis, Characterization and Catalytic Dehydration of Glycerol to Acrolein Over Phosphotungstic Acid Supported Y-Zeolite Catalysts, Catal. Lett. 148 (2018) 397–406, https://doi.org/10.1007/s10562-017-2236-9.

[25] E. Kraleva, H. Atia Keggin, Type Heteropolyacids Supported on Sol-Gel Oxides as Catalysts For the Dehydration of Glycerol to Acrolein, React. Kinet. Mech. Catal. 126 (2019) 103–117, https://doi.org/10.1007/s11144-018-1471-4.

[26] B. Viswanadham, V. Vishwanathan, K.V.R. Chary, Y. Satyanarayana, Catalytic Dehydration of Glycerol to Acrolein Over Mesoporous MCM-41 Supported Heteropolyacid Catalyts, J. Porous Mater. 28 (2021) 1269–1279, https://doi.org/10.1007/s10934-021-01070-8.

[27] M.H. Haider, N.F. Dummer, D. Zhang, P. Miedziak, T.E. Davies, S.H. Taylor, D. J. Willock, D.W. Knight, D. Chadwick, G.J. Hutchings, Rubidium- and Caesium-Doped Silicotungstic Acid Catalysts Supported on Alumina for the Catalytic Dehydration of Glycerol to Alumina, J. Catal. 286 (2012) 206–213, https://doi.org/10.1016/j.jcat.2011.11.004.

[28] M.H. Haider, C. D'Agostino, N.F. Dummer, M.D. Mantle, L.F. Gladden, D. W. Knight, D.J. Willock, D.J. Morgan, S.H. Taylor, G.j. Hutchings, The Effect of Grafting Zirconia and Ceria onto Alumina as a Support for Silicotungstic Acid for the Catalytic Dehydration of Glycerol to Acrolein, Chem. Eur. J. 20 (2014) 1743–1752, https://doi.org/10.1002/chem.201302348.

[29] J. Mitchell, D.A. Graf von der Schulenberg, D.J. Holland, E.J. Fordham, M.L. Johns, L.F. Gladden, Determining NMR flow propagator moments in porous rocks without the influence of relaxation, J. Magn. Reson. 193 (2008) 218–225, https://doi.org/10.1016/j.jmr.2008.05.001.

[30] M.T. Ravanchi, M.R. Fard, S. Fadaeerayeni, F. Yaripour, Effect of Calcination Conditions on Crystalline Structure and Pore Size Distribution for a Mesoporous Alumina, Chem. Eng. Comm. 4 (2015) 493–499, https://doi.org/10.1080/00986445.2013.850577.

[31] L. Forster, M. Lutecki, H. Fordsmand, L. Yu, C. D'Agsotino, Tailoring Morphology of Hierarchical Catalysts for Tuning Pore Diffusion Behaviour: A Rational Guideline Exploiting Bench-Top Pulsed-Field Gradient (PFG) Nuclear Magnetic Resonance (NMR), Mol. Syst. Des. Eng 5 (2020) 1193–1204, https://doi.org/10.1039/D0ME00036A.

[32] R. Thouvenout, M. Fournier, R. Franck, C. Rocchiccioli-Deltcheff, Vibrational Investigations of Polyoxometalates. 3. Isomerism in Molybdenum (VI) and Tungsten (VI) Compounds Related to the Keggin Structure, Inorg. Chem. 23 (1984) 598–605, https://doi.org/10.1021/ic00173a022.

[33] S.-H. Chai, H.-P. Wang, Y. Liang, B.-q. Xu, Sustainable Production of Acrolein: Preparation and Characterization of Zirconia-Supported 12-Tungstophosphoric Acid Catalyst for Gas-Phase Dehydration of Glycerol, Appl. Catal. A-Gen. 353 (2009) 213–222, https://doi.org/10.1016/j.apcata.2008.10.040.

[34] G. Filippini, F. Longobardo, L. Forster, A. Criado, G. Di Carmine, L. Nasi, C. D'Agostino, M. Melchionna, P. Fornasiero, M. Prato, Light-Driven, Heterogeneous Organocatalysts for C-C Bond Formation Toward Valuable Perfluoroalkylated Intermediates, Sci. Adv. 6 (2020), Article eabc9923, 10.1126/sciadv.abc9923.

[35] L. Forster, C. D'Agostino, M.A. Llosa-Tanco, V. Spallina, C. Brencio, F. Gallucci, M. Lindley, S.J. Haigh, D.a. Pacheco-Tanaka, Tailoring Pore Structure and Surface Chemistry of Microporous Alumina-Carbon Molecular Sieve Membranes (Al-CMSMs) by Altering Carbonization Temperature for Optimal Gas Separation Performance: An Investigation Using Low-Field NMR Relaxation Measurements, Chem. Eng. J. 424 (2021), 129313, https://doi.org/10.1016/j.cej.2021.129313.

[36] M.R. Barr, L. Forster, C. D'Agostino, R. Volpe, Alkaline Pretreatment of Walnut Shells Increases Pore Surface Hydrophilicity of Derived Biochars, Appl. Surf. Sci. 571 (2022), 151253, https://doi.org/10.1016/j.apsusc.2021.151253.

[37] G. Di Carmine, L. Forster, S. Wang, C. Parlett, A. Carlone, C. D'Agostino, NMR Relaxation Time Measurements of Solvent Effects in an Organocatalysed Asymmetric Aldol Reaction over Silica SBA-15 Supported Proline, React. Chem. Eng. 7 (2022) 269–274, https://doi.org/10.1039/D1RE00471A.

[38] N. Robinson, C. Robertson, L.F. Gladden, S.J. Jenkins, C. D'Agostino, Direct Correlation between Adsorption Energetics and Nuclear Spin Relaxation in a Liquid-Saturated Catalyst Material, ChemPhysChem 19 (2018) 2472–2479, https://doi.org/10.1002/cphc.201800513.

[39] N. Robinson, P. Bräuer, A.P.E. York, C. D'Agostino, Nuclear Spin Relaxation as a Probe of Zeolite Acidity: A Combined NMR and TPD Investigation of Pyridine in HZSM-5, Phys. Chem. Chem. Phys. 23 (2021) 17752–17760, https://doi.org/10.1039/D1CP01515J.

[40] C. D'Agostino, A.P.E. York, P. Bräuer, Host-Guest Interaction and Confinement Effects in HZSM-5 and Chabazite Zeolites Studied by Low-Field NMR Spin Relaxation, Mater. Today Chem. 24 (2022), Article 100901, 10.1016/j.mtchem.2022.100901.

[41] A. Platon, W.j. Thomson, Quantitative Lewis/Brønsted Ratios Using DRIFTS, Ind. Eng. Chem. Res. 42 (2003) 5988–5992, https://doi.org/10.1021/ie030343g.

[42] E. Selli, L. Forni, Comparison Between the Surface Acidity of Solid Catalysts Determined by TPD and FTIR Analysis of Pre-Adsorbed Pyridine, Microporous Mesoporous Mater. 31 (1999) 129–140, https://doi.org/10.1016/S1387-1811(99)00063-3.

[43] B.T. Loveless, A. Gyanani, D.s. Muggli, Discrepancy Between TPD- and FTIR-Based Measurements of Brønsted and Lewis Acidity for Sulfated Zirconia, Appl. Catal. B 84 (2008) 591–597, https://doi.org/10.1016/j.apcatb.2008.05.025.

[44] C. D'Agostino, J. Mitchell, M.D. Mantle, L. f. Gladden, Interpretation of NMR Relaxation as a Tool for Characterising the Adsorption Strength of Liquids inside Porous Materials, Chem. Eur. J. 20 (2014) 13009–13015, https://doi.org/10.1002/chem.201403139.

[45] D. Weber, J. Mitchell, J. McGregor, L.F. Gladden, Comparing Strengths of Surface Interactions for Reactants and Solvents in Porous Catalysts Using Two-Dimensional NMR Relaxation Correlations, J. Phys. Chem. C 113 (16) (2009) 6610–6615.

[46] X. Yang, Z. Sun, D. Wang, W. Forsling, Surface Acid-Base Properties and Hydration/Dehydration Mechanisms of Aluminium (Hydr)oxides, J. Colloid Interface Sci. 308 (2007) 395–404, https://doi.org/10.1016/j.jcis.2006.12.023.

[47] B. Katryniok, S. Paul, M. Capron, C. Lancelot, V. Billiére-Baca, P. Rey, F. Dumeignil, A Long Life Catalyst for Glycerol Dehydration to Glycerol, Green Chem. 12 (2010) 1922–1925, https://doi.org/10.1039/c0gc00254b.

[48] Y. Wu, X. Ye, X. Yang, X. Wang, W. Chu, Y. Hu, Heterogenization of Heteropolyacids: A General Discussion on the Preparation of Supported Acid Catalysts, Ind. Eng. Chem. Res. 35 (1996) 2546–2560, https://doi.org/10.1021/ie950473s.

[49] S.-H. Chai, H.-P. Wang, Y. Liang, B.-q. Xu, Sustainable Production of Acrolein: Investigation of Solid Acid-Base Catalysts for Gas-Phase Dehydration of Glycerol, Green Chem. 9 (2007) 1130–1136, https://doi.org/10.1039/b702200j.

[50] S.-H. Chai, H.-P. Wang, Y. Liang, B.-q. Xu, Sustainable Production of Acrolein: Gas-Phase Dehydration of Glycerol Over Nb_2O_5 Catalyst, J. Catal. 250 (2007) 342–349, https://doi.org/10.1016/j.jcat.2007.06.016.

[51] B. Djuricic, S. Pickering, P. Glaude, D. McGarry, P. Tambusyer, Thermal Stability of Transition Phases in Zirconia-Doped Alumina, J. Mater. Sci. 32 (1997) 589–601, https://doi.org/10.1023/A:1018567230733.

[52] T. Horiuchi, Y. Teshima, T. Osaki, T. Sugiyama, K. Suzuki, T. Mori, Improvement of Thermal Stability by Addition of Zirconia, Catal. Lett. 62 (1999) 107–111, https://doi.org/10.1023/A:1019051123075.